PHYSICAL REVIEW B **89**, 241303(R) (2014)

Strain-induced active tuning of the coherent tunneling in quantum dot molecules

E. Zallo,[1,*] R. Trotta,[1,2] V. Křápek,[3] Y. H. Huo,[1] P. Atkinson,[4] F. Ding,[1] T. Šikola,[3] A. Rastelli,[1,2] and O. G. Schmidt[1,5,6]
[1] *Institute for Integrative Nanosciences, IFW Dresden, Helmholtzstrasse 20, D-01069 Dresden, Germany*
[2] *Institute of Semiconductor and Solid State Physics, Johannes Kepler University Linz, Altenbergerstrasse 69, A-4040 Linz, Austria*
[3] *Central European Institute of Technology, Brno University of Technology, Technická 10, CZ-61600 Brno, Czech Republic*
[4] *Sorbonne Universités, UPMC Université Paris 06, CNRS, UMR 7588, INSP, 4 place Jussieu, F-75005 Paris, France*
[5] *Material Systems for Nanoelectronics, Technische Universität Chemnitz, Reichenhainerstrasse 70, D-09107 Chemnitz, Germany*
[6] *Center for Advancing Electronics Dresden, Technische Universität Dresden, Georg-Schumannstrasse 11, D-01187 Dresden, Germany*
(Received 13 November 2013; revised manuscript received 12 May 2014; published 19 June 2014)

We demonstrate experimentally the possibility to manipulate the coupling strength in an asymmetric pair of electronically coupled InGaAs quantum dots by using externally induced strain fields. The coupling strength of holes confined in the dots increases linearly with increasing tensile strain. A model based on $\boldsymbol{k}\cdot\boldsymbol{p}$ theory explains the effect in terms of modified weight of the light hole component mediating the coupling in the barrier. Our results are relevant to the creation and control of entangled states in optically active quantum dots.

DOI: 10.1103/PhysRevB.89.241303 PACS number(s): 78.67.Hc, 78.20.hb, 78.55.Cr, 85.35.Be

A quantum dot molecule (QDM)—two semiconductor QDs separated by a thin barrier—represents a striking example of the analogy between artificial and natural atomic combinations. Similar to the energy levels in a hydrogen molecule, bonding and antibonding states are formed via coherent tunneling [1] of charges in a QDM, giving rise to anticrossing (AC) patterns in the electric-field dependent photoluminescence (PL) spectra [2–5]. This artificial quantum system has a potential application as a quantum gate in quantum information processing [6–8], mainly due to the possibility to initialize and control entanglement between solid-state qubits [9–13]. Although the fine structure of the optical spectra and the spin properties of QDMs made of two vertically stacked InGaAs QDs in a GaAs matrix are now well understood [11,14–16], active control of the coupling strength between the two QDs—the key parameter determining the operation rate of quantum gates [9,10]—still needs to be demonstrated. In particular, the probability of a Landau-Zener transition [17] (the transition from one AC branch to the other), important in qubit manipulation [10], increases exponentially as the coupling strength is decreased. Some qubit proposals [1] also require comparable electron and hole tunneling rates [13]. Contrary to (optically inactive) electrostatically defined QDMs [18,19], the spacer thickness in vertical QDMs is frozen and there is no growth protocol [20] allowing an active control over the spin qubit. A postgrowth tuning of the coherent tunneling would overcome this shortcoming. Longitudinal or transverse magnetic fields were predicted to affect the coupling strength in vertical QDMs [21–24], but more recent experiments and refined theoretical treatments have shown no significant changes for fields up to 6 T [25]. Therefore, it remains unclear if and how the tunneling rate of carriers in a vertical QDM can be tuned.

In this Rapid Communication, we demonstrate active tuning of the coupling strength of holes confined in individual InGaAs/GaAs QDMs by externally induced strains. Eight-band $\boldsymbol{k}\cdot\boldsymbol{p}$ calculations reveal that the origin of the observed effect is a strain-induced modification of the heavy hole (HH) and light hole (LH) effective confinement potentials, which in turn change the probability density for the hole states and thus the coupling strength between the dots.

The device design employed in this work [26,27] allows large stress and electric fields to be applied to single QDMs. The QDMs consist of two vertically stacked InGaAs QDs [28] embedded in the intrinsic region of n-i-p nanomembranes integrated onto piezoelectric actuators made of lead magnesium niobate–lead titanate (PMN-PT); see Fig. 1(a). The QDs are grown on a semi-insulating GaAs (001) substrate by molecular beam epitaxy at the center of a 10 nm thick $GaAs/Al_{0.4}Ga_{0.6}As$ quantum well, in order to reduce carrier escape at high electric fields (F_d) across the diode [29]. The QD height, which has a major influence on the confinement energy, was controlled by means of the *indium flush* method [30]. The different confined energy levels in the two dots are tuned into resonance by applying a voltage (V_d) across the nanomembranes. Simultaneously, in-plane (compressive or tensile) biaxial stress is transferred to the QD layers [31] by applying a voltage (V_p) across the PMN-PT. While piezoelectric-induced strains have been used previously to control several properties of semiconductor structures [32–36], their potential in the field of QDMs still needs to be explored. The micro-PL (μPL) measurements were performed at 6 K in a helium flow cryostat with a 50× microscope objective (numerical aperture = 0.42). The device was excited with a 532 nm continuous-wave laser and the signal was collected by the same microscope objective used for the excitation and analyzed by a single (double) spectrometer featuring ~30 μeV (~15 μeV) spectral resolution. The degree of linear polarization of the PL signal was analyzed by combining a rotatable achromatic half-wave plate and a fixed linear polarizer. For more details see the Supplemental Material [37].

Figure 1(b) shows the simultaneous effect of electric and strain fields on a representative InGaAs QDM. By sweeping the electric field across the diode (F_d in $[-14.4,-6.5]$ kV/cm), the X-shaped pattern of the positively charged exciton (X^+) [4] can be clearly observed. The magnitude of AC energy gaps (ΔE_{AC}) [20], defined as the minimum energy splitting between bonding and antibonding states, and polarized cross-correlation measurements between X^+ and X^0 [38] confirm

*e.zallo@ifw-dresden.de

 ©2014 American Physical Society

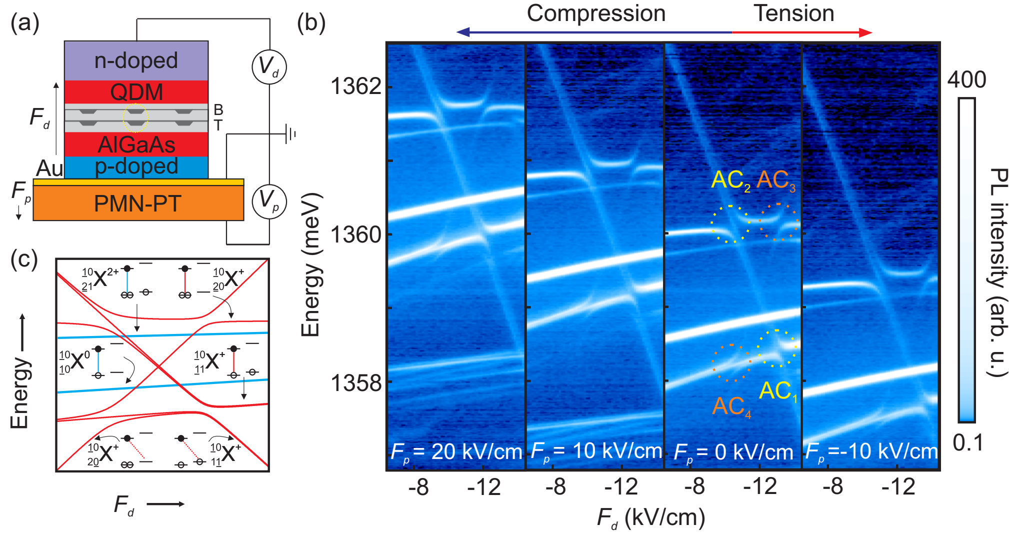

FIG. 1. (Color online) (a) Sketch of the device. Vertically stacked, disk-shaped InGaAs QDs (bottom-B/top-T QD with a nominal height of 2.9/3.3 nm and a spacer thickness of 5.4 nm) are embedded in n-i-p nanomembranes integrated on top of a piezoelectric actuator (PMN-PT) allowing in situ application of biaxial stresses by tuning the voltage (electric field) V_p (F_p). Independently, a voltage V_d applied to the nanomembranes allows the electric field (F_d) across the QDs to be controlled. (b) Color-coded microphotoluminescence (μPL) maps of a representative QDM as a function of F_p and F_d (PL intensity in logarithmic scale). The typical anticrossings observed ($AC_{1\text{–}4}$) are associated with hole tunneling and are marked on the map at $F_p = 0$ kV/cm. (c) Sketch of the transition energies of the positively charged (X^+) and neutral (X^0) excitons in a QDM (the X^+ pattern is obtained by the formula reported in the Supplemental Material [37]). By sweeping F_d, different transitions are defined: two direct ($^{10}_{20}X^+$ and $^{10}_{11}X^+$) and two indirect ($^{10}_{11}X^+$ and $^{10}_{20}X^+$) with a larger Stark shift. The two additional lines are direct recombinations arising from the neutral exciton ($^{10}_{10}X^0$) and the doubly positively charged exciton ($^{10}_{21}X^{2+}$).

this identification. The typical behavior of the excitonic energy levels as a function of the electric field is sketched in Fig. 1(c). As in Ref. [4], we consider transitions between the initial (X^+) and the final (single hole) states. Two indirect transitions, $^{10}_{11}X^+$ and $^{10}_{20}X^+$, where electrons and holes recombine in different dots, anticross two direct transitions, $^{10}_{20}X^+$ and $^{10}_{11}X^+$, where the recombination takes place in the same dot [39]. The ACs have a magnitude ranging between 0.2 and 0.4 meV, reflecting the overlap of the charge carrier wave functions in the interdot region [1], and appear at different F_d because of different Coulomb interaction values. The AC_1 and AC_2 (see the map at the strain field $F_p = 0$ kV/cm) represent the anticrossing of $^{10}_{11}X^+$ and $^{10}_{20}X^+$, respectively, with $^{10}_{11}X^+$. The AC_3 and AC_4 are obtained by the anticrossing of the direct trion recombinations with the weak transition $^{10}_{20}X^+$, theoretically forbidden because of no holes in the final state but partially tunnel induced in the experiment. The lines going through AC_2 and AC_4 have previously been assigned to the spin triplet configuration of the two holes in X^+ due to Pauli blocking [15,40], because tunneling conserves spin and the anticrossing lines represent singlet spin states. Indirect transitions show more pronounced Stark shifts (the change in energy with electric field) than direct excitons due to their larger static electric dipole. From the slope of the energy of the indirect transitions with respect to F_d we infer an electron-hole (e-h) average distance of ~7 nm, in reasonable agreement with the nominal center-to-center dot separation ($d = 8.5$ nm). Two additional direct recombination lines are observed in the spectra: The brightest line stems from the neutral exciton, $^{10}_{10}X^0$, and the weak line from the doubly positively charged exciton, $^{10}_{21}X^{2+}$. From the slope of the direct transition we obtain a permanent exciton dipole ~0.48 e nm, where the positive sign means that the electron wave function is shifted towards the dot apex, possibly due to local In enrichment [41].

In the following we focus on the strain effects on the coupling signature of the X^+. When biaxial stress is applied to the nanomembrane, the spectrum changes significantly. The PL emission lines blueshift (redshift) for positive (negative) F_p, due to compressive (tensile) strain [35,36]. At the same time the values of F_d at which ACs occur increase (decrease) under compressive (tensile) strain, as predicted in Ref. [42]. By comparison with previous work [27], we estimate that in-plane strain transferred to the GaAs nanomembrane varies by about 0.06%, when F_p is swept through the whole tuning range ($\Delta F_p = 30$ kV/cm), and the corresponding energy shift of the neutral exciton (ΔE_p) is about 2.4 meV.

The most important result of this work is revealed by the higher resolution μPL spectra of the same QDM, shown in Fig. 2. In Figs. 2(a) and 2(b) we compare the region of AC_1 at the highest and lowest F_p (20 and −10 kV/cm), corresponding respectively to the highest value of compressive and tensile strains achieved in our device. We observe that application of compressive (tensile) stress leads to a reduction (increase) of the tunnel coupling. In particular, we measure a linear increase of ΔE_{AC_1} by 27 μeV for $\Delta E_p = 2.4$ meV [see Fig. 2(f)], where ΔE_{AC_1} was obtained by fitting the energy splitting between bonding and antibonding states (ΔE) as a function of F_d [see Fig. 2(e)]. For details about the fitting procedure, see Ref. [37]. A more pronounced effect was measured for AC_2 with a tuning range of 48 μeV in the same interval of fields, as shown in Figs. 2(c), 2(d), and 2(f). Therefore, our data clearly demonstrate that the combination of strain and

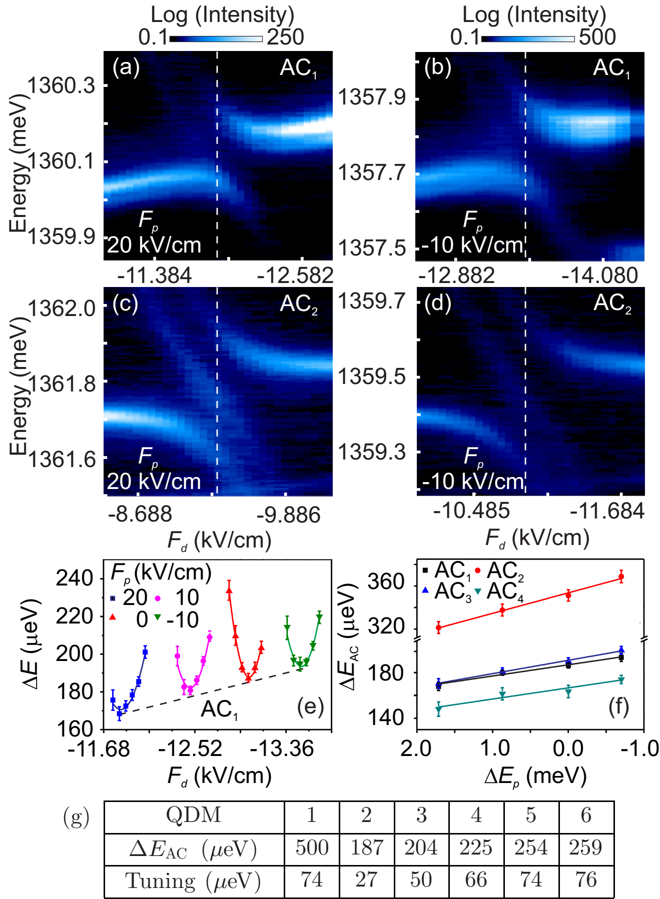

QDM	1	2	3	4	5	6
ΔE_{AC} (μeV)	500	187	204	225	254	259
Tuning (μeV)	74	27	50	66	74	76

FIG. 2. (Color online) Color-coded μPL maps of the (a), (b) AC_1 and (c), (d) AC_2 regions as a function of F_d at $F_p = 20$ kV/cm (compressive strain, -0.04%) and $F_p = -10$ kV/cm (tensile strain, 0.02%), respectively. The dashed line marks the AC position. (e) Parabolic behavior of the energy splitting (ΔE) between the bonding and antibonding molecular states around AC_1 as a function of F_d at $F_p = 20$, 10, 0, -10 kV/cm. (f) Behavior of ΔE_{AC} at $\mathrm{AC}_{1\text{–}4}$ as a function of the neutral exciton PL energy shift (ΔE_p), when F_p is varied through the whole tuning range ($\Delta F_p = 30$ kV/cm). (g) ΔE_{AC} and the tuning range of the coupling strength in the range $F_p = 20$ to -10 kV/cm for six QDMs.

electric fields allows the coupling strength of the QDM to be actively manipulated.

Very similar results were obtained in six other QDMs chosen randomly in our device; see Fig. 2(g). Specifically, we find that ΔE_{AC} fluctuates between different QDMs with an average value of (270 ± 120) μeV. This is due to fluctuations over the size, shape, and composition among the different QDs and it is related to the lack of control over the QD growth processes. On the other hand, the effect of the induced strain is quite similar for all the investigated QDMs, with an average value of (61 ± 19) μeV. We argue that by increasing the strain induced in the membrane up to 0.4%, as obtained in Ref. [27], we would be able to obtain the same predefined coupling strength for any QDM in our sample (see Ref. [37] for details).

From the linear fit of the ΔE_{AC} as a function of ΔE_p we obtain a slope ratio $\alpha(\mathrm{AC}_2)/\alpha(\mathrm{AC}_1) = 1.9$. This result is consistent with the coupling dynamics obtained by the formula $\Delta E_{\mathrm{AC}_2} = \sqrt{2}\Delta E_{\mathrm{AC}_1}\sqrt{1 + 2J_{eh}^2/\Delta E_{\mathrm{AC}_1}^2}$ as reported in Ref. [15], where J_{eh} is the *e-h* exchange energy [16] and the factor $\sqrt{2}$ considers the tunneling of two holes between the two dots. The unpaired hole spin of ${}^{10}_{11}X^+$ results in the doublet structure of intense lines in Figs. 2(a) and 2(b) with the splitting increasing with tensile strain. Moreover, the line that passes almost unaffected through AC_2 at the resonance point is no longer in the center and its energy separation from the antibonding branch (higher energy component) is slightly increased, as shown in Figs. 2(c) and 2(d). This reflects a different influence of strain on the triplet and singlet states. A similar strain effect on the coupling strength is measured on all the other anticrossings [see Fig. 2(f) and Ref. [37] for details].

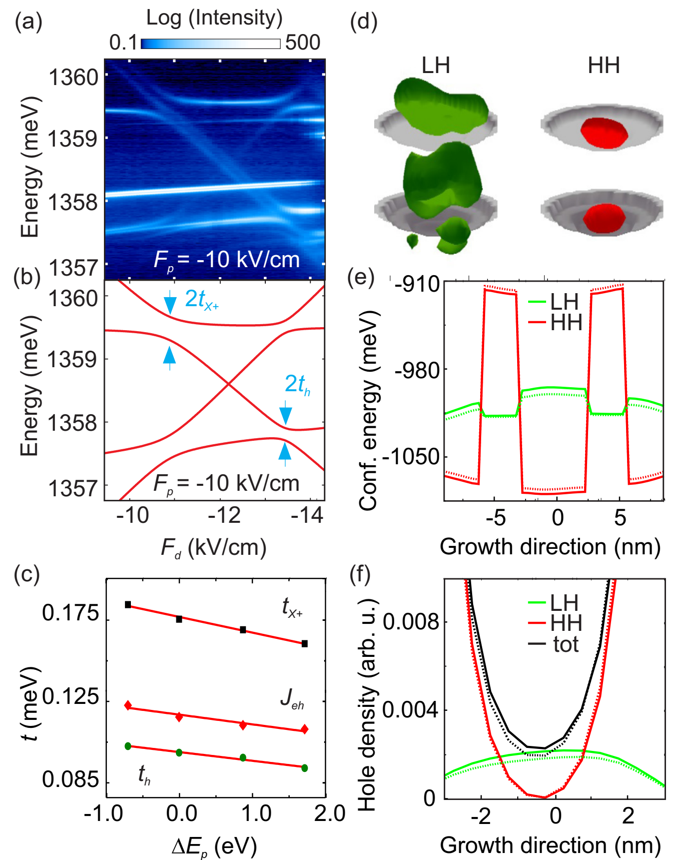

FIG. 3. (Color online) (a) Color-coded μPL map of a representative QDM as a function of F_d at $F_p = -10$ kV/cm. (b) Transition energies of X^+ in the QDM (AC lines) resulting from a fit to the experimental spectrum of (a). All the parameters used to fit the data are listed in Table S1 [37]. (c) Tunneling energies of single hole (t_h) and X^+ (t_{X^+}) and electron-hole exchange interaction (J_{eh}) as a function of ΔE_p, when F_p is varied in the whole range. (d) Three-dimensional hole probability density of light hole (LH, green) and heavy hole (HH, red) in the QDM (gray). The center-to-center dot separation is 8.5 nm. (e) Confinement potentials of LH (green) and HH (red) for the structure without (solid) and with induced compressive strain of $\epsilon_{xx} = \epsilon_{yy} = -0.1\%$ (dotted). Energy is displayed in the electron view. (f) Hole probability density in the barrier region of LH (green), HH (red), and total (black) for the unstrained (solid) and strained (dotted) case.

In order to extract the relevant parameters of the QDM and their evolution upon application of stress, we describe the system with a modified Hamiltonian from the model reported in Ref. [4], by taking into account the Stark shifts of the direct transitions. We consider the transitions between the initial state with one electron and two holes ($\hat{H}_{X^+}$) and the final state with a single hole ($\hat{H}_h$) focusing on the four lines that anticross each other and neglecting the spin-exchange interaction; see Ref. [37]. The pattern is obtained by diagonalizing the two matrices,

$$\hat{H}_{X^+}^{(2\times2)} = \begin{pmatrix} \Gamma^{(-)} & -t_{X^+} \\ -t_{X^+} & -F'_d d^*_{X^+} \end{pmatrix}, \quad \hat{H}_h = \begin{pmatrix} \epsilon_h & -t_h \\ -t_h & \epsilon_h - F'_d d^*_h \end{pmatrix},$$

where $\hat{H}_{X^+}^{(2\times2)}$ is the reduced Hamiltonian of the singlet states, $\Gamma^{(-)}$ is the energy distance between ${}^{10}_{20}X^+$ and ${}^{10}_{11}X^+$, $t = \Delta E_{\rm AC}/2$ is the tunneling energy, F'_d is the electric field ($F'_d = 0$ at AC$_1$), d^* is the effective interdot distance, and ϵ_h is the ground state energy of the hole. Finally, the energy differences $E_{1,2}[\hat{H}_{X^+}^{(2\times2)}] - E_{1,2}[\hat{H}_h]$ provide the pattern plotted in Fig. 3(b) at $F_p = -10$ kV/cm, which fits the experimental data reported in Fig. 3(a). The fitting parameters are $\Gamma^{(-)}$, d^*_h, $d^*_{X^+}$, $\Delta E_{\rm AC_1} = 2t_h$, and $\Delta E_{\rm AC_2} = 2t_{X^+}$. Under compression both t_h and t_{X^+} decrease linearly as a function of ΔE_p; see Fig. 3(c). Using the same formula reported above linking t_h and t_{X^+}, we found that $J_{eh} \sim 115$ μeV at $F_p = 0$ kV/cm, consistent with singlet-triplet splittings measured in similar structures [16], and it decreases with compressive strain. Additional information is obtained by looking at the screening, that is, the difference $d - d^*$, as a function of ΔE_p; see Ref. [37]. This difference at $F_p = 0$ kV/cm for the initial state (X^+) is ~11% larger with respect to the final state (single hole) because of the extra *e*-*h* pair.

In order to understand the physical origin of the observed changes in $\Delta E_{\rm AC}$, we calculated the electronic structure and the optical properties of the studied QDMs using the eight-band $\boldsymbol{k}\cdot\boldsymbol{p}$ calculations including realistic strain distribution and piezoelectric field; see Ref. [37] (see also Refs. [3,4] therein). For the system under study with $F_p = 0$ kV/cm, we obtain a transition energy ~1.37 eV for the neutral exciton, an energy difference between the symmetric and antisymmetric states $\Delta E_{\rm AC_1}$ of 284 μeV, and a decrease of 46 μeV in the tunnel coupling while sweeping the externally induced strain from tensile 0.02% to compressive −0.04%, in agreement with the experimental results [43]. Inspection of the wave functions reveals that the hole probability density in the barrier region is dominated by the LH component, as shown in Figs. 3(d) and 3(f), Refs. [13] and [44]. This is because the band edge of LHs in the GaAs barrier is about 80 meV below the HH band edge, due to the local tensile strain induced by the QDs. The HHs penetrate the barrier region only by exponentially decaying tails at the QD boundaries, leaving negligible probability density in the barrier center. The compressive strain increases the energy of LHs with respect to the HHs [see Fig. 3(e)], leading to a reduction of the LH component in the barrier and therefore the tunnel coupling. We note that reducing the center-to-center dot separation below 8 nm will promote the HHs in the barrier region eventually leading to the opposite dependence of $\Delta E_{\rm AC_1}$ on strain, i.e., increase of tunnel coupling upon lateral compression.

In conclusion, we have demonstrated that externally induced strains can be employed to tune the coupling strength in single InGaAs/GaAs QDMs. The strain changes the effective confinement potential of the HH and LH in the barrier and dot region, resulting in the reduction of the hole tunneling for compressive strain. By applying electric and strain fields, $\Delta E_{\rm AC_1}$ is varied up to 27 μeV and $\Delta E_{\rm AC_2}$ up to 48 μeV. This achievement may pave the way to a precise and flexible control of the entanglement between solid-state spin qubits in optically active QDMs. We envision using the strain field to tune the coupling strength of different QDMs to predetermined reference values combined with fast electric pulses across the device [45] to both initialize and readout the desired delocalized QDM states. Faster control may be achieved by strain modulations of the coupling strength provided by surface acoustic waves [46–48].

We thank C. Ortix, D. Gammon, S. Kumar, G. Bester, and J. Zhang for fruitful discussions, B. Eichler, D. J. Thurmer, R. Engelhardt, and D. Grimm for technical support, and K. Dörr and A. Herklotz for help with the piezoelectric actuators. The work was financially supported by the BMBF project QuaHL-Rep (Contracts No. 01BQ1032 and No. 01BQ1034), the DFG (FOR 730, contract RA1634/1-1), and the European Union Seventh Framework Programme 209 (FP7/2007-2013) under Grant Agreement No. 601126 210 (HANAS). V.K. was supported by European Social Fund, Grant No. CZ.1.07/2.3.00/30.0005. T.Š. was supported by European Regional Development Fund, Project No. CZ.1.05/1.1.00/02.0068.

[1] M. Bayer, P. Hawrylak, K. Hinzer, S. Fafard, M. Korkusinski, Z. R. Wasilewski, O. Stern, and A. Forchel, Science **291**, 451 (2001).

[2] H. J. Krenner, M. Sabathil, E. C. Clark, A. Kress, D. Schuh, M. Bichler, G. Abstreiter, and J. J. Finley, Phys. Rev. Lett. **94**, 057402 (2005).

[3] G. Ortner, M. Bayer, Y. Lyanda-Geller, T. L. Reinecke, A. Kress, J. P. Reithmaier, and A. Forchel, Phys. Rev. Lett. **94**, 157401 (2005).

[4] E. A. Stinaff, M. Scheibner, A. S. Bracker, I. V. Ponomarev, V. L. Korenev, M. E. Ware, M. F. Doty, T. L. Reinecke, and D. Gammon, Science **311**, 636 (2006).

[5] A. Boyer de la Giroday, N. Sköld, I. Farrer, D. A. Ritchie, and A. J. Shields, J. Appl. Phys. **110**, 083511 (2011).

[6] D. Loss and D. P. DiVincenzo, Phys. Rev. A **57**, 120 (1998).

[7] J. R. Petta, A. C. Johnson, J. M. Taylor, E. A. Laird, A. Yacoby, M. D. Lukin, C. M. Marcus, M. P. Hanson, and A. C. Gossard, Science **309**, 2180 (2005).

[8] L. Robledo, J. Elzerman, G. Jundt, M. Atatüre, A. Högele, S. Fält, and A. Imamoğlu, Science **320**, 772 (2008).
[9] D. Kim, S. G. Carter, A. Greilich, A. S. Bracker, and D. Gammon, Nat. Phys. **7**, 223 (2011).
[10] G. Cao, H.-O. Li, T. Tu, L. Wang, C. Zhou, M. Xiao, G.-C. Guo, H.-W. Jiang, and G.-P. Guo, Nat. Commun. **4**, 1401 (2013).
[11] K. M. Weiss, J. M. Elzerman, Y. L. Delley, J. Miguel-Sanchez, and A. Imamoğlu, Phys. Rev. Lett. **109**, 107401 (2012).
[12] A. Greilich, S. G. Carter, D. Kim, A. S. Bracker, and D. Gammon, Nat. Photonics **5**, 702 (2011).
[13] G. Bester, A. Zunger, and J. Shumway, Phys. Rev. B **71**, 075325 (2005).
[14] M. F. Doty, J. I. Climente, M. Korkusinski, M. Scheibner, A. S. Bracker, P. Hawrylak, and D. Gammon, Phys. Rev. Lett. **102**, 047401 (2009).
[15] M. Scheibner, M. F. Doty, I. V. Ponomarev, A. S. Bracker, E. A. Stinaff, V. L. Korenev, T. L. Reinecke, and D. Gammon, Phys. Rev. B **75**, 245318 (2007).
[16] A. Greilich, Ş. C. Bădescu, D. Kim, A. S. Bracker, and D. Gammon, Phys. Rev. Lett. **110**, 117402 (2013).
[17] C. Zener, Proc. R. Soc. London, Ser. A **137**, 696 (1932).
[18] A. K. Hüttel, S. Ludwig, H. Lorenz, K. Eberl, and J. P. Kotthaus, Phys. Rev. B **72**, 081310(R) (2005).
[19] Y. Hu, H. O. H. Churchill, D. J. Reilly, J. Xiang, C. M. Lieber, and C. M. Marcus, Nat. Nanotechnol. **2**, 622 (2007).
[20] A. S. Bracker, M. Scheibner, M. F. Doty, E. A. Stinaff, I. V. Ponomarev, J. C. Kim, L. J. Whitman, T. L. Reinecke, and D. Gammon, Appl. Phys. Lett. **89**, 233110 (2006).
[21] G. Burkard, G. Seelig, and D. Loss, Phys. Rev. B **62**, 2581 (2000).
[22] M. Korkusiński and P. Hawrylak, Phys. Rev. B **63**, 195311 (2001).
[23] L. G. G. V. Dias da Silva, J. M. Villas-Bôas, and S. E. Ulloa, Phys. Rev. B **76**, 155306 (2007).
[24] J. J. Climente, Appl. Phys. Lett. **93**, 223109 (2008).
[25] J. Planelles, J. I. Climente, F. Rajadell, M. F. Doty, A. S. Bracker, and D. Gammon, Phys. Rev. B **82**, 155307 (2010).
[26] R. Trotta, E. Zallo, C. Ortix, P. Atkinson, J. D. Plumhof, J. van den Brink, A. Rastelli, and O. G. Schmidt, Phys. Rev. Lett. **109**, 147401 (2012).
[27] R. Trotta, P. Atkinson, J. D. Plumhof, E. Zallo, R. O. Rezaev, S. Kumar, S. Baunack, J. R. Schröter, A. Rastelli, and O. G. Schmidt, Adv. Mater. **24**, 2668 (2012).
[28] Q. Xie, A. Madhukar, P. Chen, and N. P. Kobayashi, Phys. Rev. Lett. **75**, 2542 (1995).
[29] A. J. Bennett *et al.*, Nat. Phys. **6**, 947 (2010).
[30] Z. R. Wasilewski, S. Fafard, and J. P. McCaffrey, J. Cryst. Growth **201-202**, 1131 (1999).
[31] S. Kumar, R. Trotta, E. Zallo, J. D. Plumhof, P. Atkinson, A. Rastelli, and O. G. Schmidt, Appl. Phys. Lett. **99**, 161118 (2011).
[32] C. Y. Hung, T. E. Schlesinger, and M. L. Reed, Appl. Phys. Lett. **59**, 3598 (1991).
[33] M. Shayegan, K. Karrai, Y. P. Shkolnikov, K. Vakili, E. P. De Poortere, and S. Manus, Appl. Phys. Lett. **83**, 5235 (2003).
[34] T. Gokmen, M. Padmanabhan, and M. Shayegan, Nat. Phys. **6**, 621 (2010).
[35] S. Seidl, M. Kroner, A. Högele, K. Karrai, R. J. Warburton, A. Badolato, and P. M. Petroff, Appl. Phys. Lett. **88**, 203113 (2006).
[36] F. Ding *et al.*, Phys. Rev. Lett. **104**, 067405 (2010).
[37] See Supplemental Material at http://link.aps.org/supplemental/10.1103/PhysRevB.89.241303 for experimental and theoretical details.
[38] M. H. Baier, A. Malko, E. Pelucchi, D. Y. Oberli, and E. Kapon, Phys. Rev. B **73**, 205321 (2006).
[39] The upper (lower) numbers in the notation of the quantum states are the numbers of electrons (holes) in the bottom and top dot, respectively, and the underlines represent where the recombination takes place.
[40] F. H. L. Koppens, J. A. Folk, J. M. Elzerman, R. Hanson, L. H. Willems van Beveren, I. T. Vink, H. P. Tranitz, W. Wegscheider, L. P. Kouwenhoven, and L. M. K. Vandersypen, Science **309**, 1346 (2005).
[41] P. W. Fry *et al.*, Phys. Rev. Lett. **84**, 733 (2000).
[42] J. Wang, D. Shang, H. Mao, J. Yu, Q. Zhao, P. Yang, and H. Xing, Physica B **408**, 98 (2013).
[43] The small difference between the experimental and theoretical values for the emission energy and ΔE_{AC_1} are explained by the strong dependence on structural parameters, in particular, the thickness of the spacing layer.
[44] W. Sheng and J.-P. Leburton, Appl. Phys. Lett. **81**, 4449 (2002).
[45] J. Zhang, F. Ding, E. Zallo, R. Trotta, B. Höfer, L. Han, S. Kumar, Y. H. Huo, A. Rastelli, and O. G. Schmidt, Nano Lett. **13**, 5808 (2013).
[46] J. R. Gell, M. B. Ward, R. J. Young, R. M. Stevenson, P. Atkinson, D. Anderson, G. A. C. Jones, D. A. Ritchie, and A. J. Shields, Appl. Phys. Lett. **93**, 081115 (2008).
[47] M. Metcalfe, S. M. Carr, A. Muller, G. S. Solomon, and J. Lawall, Phys. Rev. Lett. **105**, 037401 (2010).
[48] S. Völk, F. J. R. Schülein, F. Knall, D. Reuter, A. D. Wieck, T. A. Truong, H. Kim, P. M. Petroff, A. Wixforth, and H. J. Krenner, Nano Lett. **10**, 3399 (2010).